Journal of Materials Processing Technology, Volume 242, April 2017, Pages 49–59
DOI:10.1016/j.jmatprotec.2016.11.020

LASER OFFSET WELDING OF AZ31B MAGNESIUM ALLOY TO 316 STAINLESS STEEL

G. Casalino*, P. Guglielmi*, V. D. Lorusso*, M. Mortello**, P. Peyre***, D. Sorgente****

* DMMM Politecnico di Bari, Bari, Italy

**Welding Engineering Research Centre, Building 46, Cranfield University, Bedfordshire, MK43 0AL, United Kingdom

*** Processes and Engineering in Mechanics and Materials Laboratory (PIMM), CNRS-ENSAM Paristech, 151 Bd de l'Hôpital, Paris, France

**** School of Engineering, Università degli Studi della Basilicata, Via Ateneo Lucano, 10 - 85100 Potenza, Italy

ABSTRACT

In this paper, the feasibility of using a fiber laser to perform a dissimilar metal joining was explored. AZ31B magnesium and 316 stainless steel were autogenously joined in butt configuration. The weldability between different materials is often compromised by a large difference in thermal properties and poor metallurgical compatibility. Thus, the beam was focused onto the top surface of the magnesium plate, at a certain distance from the interfaces (offset), and without using any interlayer or groove preparation. Such a method was called laser offset welding (LOW). Results proved a very good capability. The ultimate tensile strength exceeded the value of 100 MPa, since a resistant and thin layer of hard intermetallic compounds is formed within the fusion zone. The rupture was observed within the magnesium side, far from the centerline. The metallurgy of fusion zone indicated the effectiveness of phases' coalescence, without mixing at liquid states. LOW was demonstrated to be a promising technique to join dissimilar metal welds, being capable to produce an effective bonding with good tensile strength.

Keywords: Laser offset welding, Magnesium alloy, Titanium alloy, dissimilar butt weld.

Published by Elsevier. This is the Author Accepted Manuscript issued with:Creative Commons Attribution Non-Commercial No Derivatives License (CC:BY:NC:ND 4.0).
The final published version (version of record) is available online at http://dx.doi.org/10.1016/j.jmatprotec.2016.11.020. Please refer to any applicable publisher terms of use.

1. INTRODUCTION

The capability to join magnesium alloys to steel will facilitate increased use of Mg alloys in the automotive and aerospace industries. The ultra-light magnesium has demonstrated outstanding potential for ultra-light metal construction design. Achieving versatile and tailored properties in one composite part is highly desirable. Hence, reliable welding process would enable broader deployment of magnesium alloys in structures that require integration with steel components for vehicle weight reduction.

The inherent characteristics of Magnesium alloys include strong tendency to oxidize, low absorptivity of laser beams, high thermal conductivities, high coefficients of thermal expansion, low melting and boiling temperatures. Moreover, wide solidification temperature ranges, high solidification shrinkage, a tendency to form low melting-point constituents, low viscosity, low surface tensions, high solubility of hydrogen in the liquid state, and absence of a color change at the melting point are landmarks of Mg and its alloys. Most of these characteristics make Mg alloys hard to be welded by laser.

In particular, Magnesium alloys can have a relatively large freezing range of about 420° to 620°C. Thus, there is considerable risk of hot-cracking during any fusion welding process. Therefore, no accepted method for metallurgical bonding is available.

Solid state joining of Mg alloys and steel was made with success using both ultrasonic (US) and friction stir welding (FSW) processes. The performance of adhesive bonds was also improved by using solid-state techniques.

Chen and Nakata studied the effect of tool geometry on microstructure and mechanical properties of friction stir lap-welded AZ31 Mg alloy and steel. Wei et al. (2012) also investigated the friction stir lap welding of magnesium alloy AZ31 and stainless steel (SUS302) and they found a shear strength of the lap joint, with maximum value closed to the shear strength of butt joint of friction stir welded magnesium alloy.

Jana et al (2010) studied FSW of AZ31 Mg alloy to steel in lap configuration, by developing the concept of using a third metal, such as Zn, at the interface to get successful results.

Elthalabawy and Khan (2011) also studied the eutectic bonding of austenitic stainless steel 316L to magnesium alloy AZ31 using a copper interlayer. In this application, the bonding took place thanks to the occurrence of solid state diffusion of Cu into the magnesium alloy, eutectic phase formation, interlayer dissolution, and isothermal solidification.

Diffusion brazing has been used to join advanced alloys by Saha and Khan (2006, 2013). This method can be a viable alternative for joining Mg alloys-steel dissimilar metals together. Yuan et al. (2013) investigated the diffusion-brazing of Mg alloy (AZ31) and stainless steel (AISI 304L) using a pure copper interlayer. They achieved joints free from defects and reported microhardness peaks in the transition zone due to Mg-Cu intermetallic formation.

Liu et al. (2012) studied the resistance spot welding (RSW) of AZ31B Mg alloy to DP600 steel using Zn interlayer in the form of Zn coated steel sheet. They found that a pre-existing transition layer of Fe_2Al_5 between the Zn coating and the steel improved wetting and bonding between the steel and the magnesium alloy. Wahba and Katayama (2012) studied the laser lap welding of 3 mm thick AZ31B magnesium alloy to 1.2 mm thick Zn-coated steel. An unstable welding process was reported due to different physical properties between the two materials (particularly in keyhole mode when the laser beam penetrates into the steel specimen).

Liu et al. (2010) investigated joining of AZ31B Mg alloy to Q235 steel with the addition of a 0.3 mm thick Sn interlayer, using the same hybrid process. The addition of Sn eliminated the gaps distributed along the fusion zone-steel interfaces as the presence of Sn improves the wettability of the Mg to the steel. Also Tan et al. (2014) proposed the dual-beam laser welding-brazing process for Magnesium alloy and stainless steel welds using a Mg-Al-Zn filler wire.

The laser brazing technology was studied both by Nasiri et al. (2015) and Naisiri and Zhou (2015). They predicted the early stage phase formation in the steel-interlayer-Mg alloy system during laser brazing, bonding mechanisms in the steel-interlayer-Mg alloy joints, and investigated the

mechanism of wetting in steel-interlayer-Mg alloy system. The benefits of using Al-12Si, Ni and Sn interlayers were also explored. Chen et al. (2016) joined Magnesium alloy and stainless steel by dual-beam laser welding-brazing process. The authors found that joints fractured at the interface or fusion zone at low/high heat input due to weak bonding or porosity formation at fusion zone. Some other authors have recently proposed the use of the fiber laser for welding dissimilar metal alloys, like Casalino et al. (2013) and Chen et al. (2011).

In this work, the dissimilar laser welding between AZ31B magnesium and 316 stainless steel, by adopting an alternative technique, was presented. Such a novel method, also referred as laser offset welding (LOW), consisted in focusing an Yb–YAG laser source onto the top surface of one of the two materials to be welded, at a specific distance from the interfaces, which is called offset. Neither interlayer nor groove preparation is necessary. This study aims to contribute to extend the adaptability of the above mentioned technique for producing various dissimilar metal welds, since previous studies, conducted by Thomashchuk et al. (2014) and Casalino et al. (2015), already demonstrated outstanding results in Al-Ti assemblies.

In the present case, the stainless steel plate, which presented higher melting point and larger laser weldability, was irradiated with high energy density in order to promote a stable keyhole mode welding. Then, the heat is transmitted to the Mg sheet without any mixing of liquid phases, leading to the formation of a very thin and regular interface along the weld centerline. The metallurgical bonding that develops during the process and the influence of some main welding conditions on the joint's strength, integrity, and microstructures were explored. The results obtained exhibited a promising feasibility of the LOW technique to produce dissimilar welds between AZ31B magnesium and 316 stainless steel, as demonstrated by good tensile properties and microstructural analysis. In spite of the challenging weldability between the two materials, the metallurgical bonding has resulted effective. Under optimal conditions, the ultimate tensile strength (UTS) even exceeded 100 MPa. This result was consistent with microstructural analysis, which exhibited the formation of a resistant and thin layer of intermetallic compounds within the fusion zone.

2. MATERIALS AND METHODS

2.1 Material properties and weld configuration

In this study, dissimilar assemblies between austenitic stainless steel AISI 316 and magnesium AZ31 sheets, were realized in butt configuration. The size of the sheets was 100 mm length by 50 mm width by 3 mm thickness. Despite the large difference in the tensile properties between the two materials, the weld was performed by adopting the same thickness for both plates. Such a choice was consistent with the main purpose of the investigation, which aimed to explore the process dynamics and the metallurgical bonding. Thus, although the structure would benefit from the use of a thinner steel plate, the priority of this study was to explore the effect of the keyhole along the overall plate thickness. The chemical composition and physical properties of the base metals are listed in tables 1 and 2, respectively.

Table 1 Chemical composition of the as-received materials (weight %).

	C	Al	Cr	Mn	Mo	Mg	Ni	Zn	P	S	Si	Fe
AISI 316	0.08	-	18	2	3	-	14	-	0.045	0.03	1	balance
AZ31	-	3.5	-	0.3	-	balance	-	0.5	-	-	0.1	0.005

Table 2 Properties of the as-received materials: ultimate tensile strength (UTS), yield stress (YS), Young module (E), elongation to fracture %(A %), Vickers microhardness (HV), thermal conductivity (K), melting point (Tm), density (ρ), specific heat capacity (c).

	UTS (MPa)	YS (MPa)	E (GPa)	A%	HV	K (W/(m.K))	Tm (°C)	ρ (g/ cm ^{3})	c (J/g°C)
AISI316	580	290	193	50	178	16.3	1370	8	0.5
AZ31	253	137	45	17	56	146	913	1.81	1.34

2.3 The welding procedure: LOW technique

The welds were produced by an innovative and promising technique, also referred as laser offset welding (LOW), in which the laser source is focused at a certain distance (offset) from the sheets' contact line. This was possible thanks to the selective and highly focused action of a disk laser, which provides for the keyhole regime fusion in the base structure of the irradiated material.

A schematic drawing of the technique is shown in figure 1.

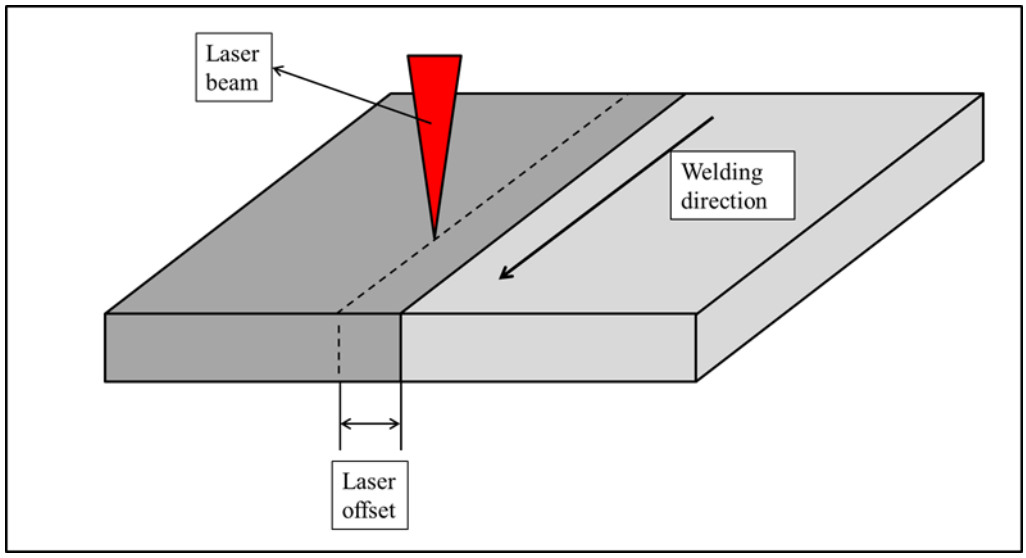


Fig.1 Schematic illustration of LOW technique procedure.

The need to explore a new procedure to build dissimilar joints derives from some drawbacks that are intrinsically related to fusion welding methods. Despite the successful outcome of traditional fusion based methods for welding a wide range of metal materials, they exhibit high weakness during dissimilar joining. On one hand, the larger the difference in thermal properties, the harder the challenge to accomplish a satisfactory weld. Further, the poor mutual solubility between different metals could hinder the formation of stable coalescence of phases. On the other hand, the formation of brittle intermetallic compounds and mixing of liquid phases weakens the mechanical properties of the joints. Moreover, vaporization phenomena occur when magnesium is irradiated by high-density energy sources. The LOW technique overcomes the limits of the previously mentioned methods, by keeping the fusion-affected interface within thin portion of material and without any direct irradiation of magnesium base sheet. The process was carried out by focusing the laser beam

on the stainless steel side, then making the keyhole to travel along a line parallel to the sheets interface. The high melting point metal is melted and then it wets the low melting point one. A thin layer of intermetallic compound forms thanks to heat propagation by conductive and convective heat transfers (see fig. 2).

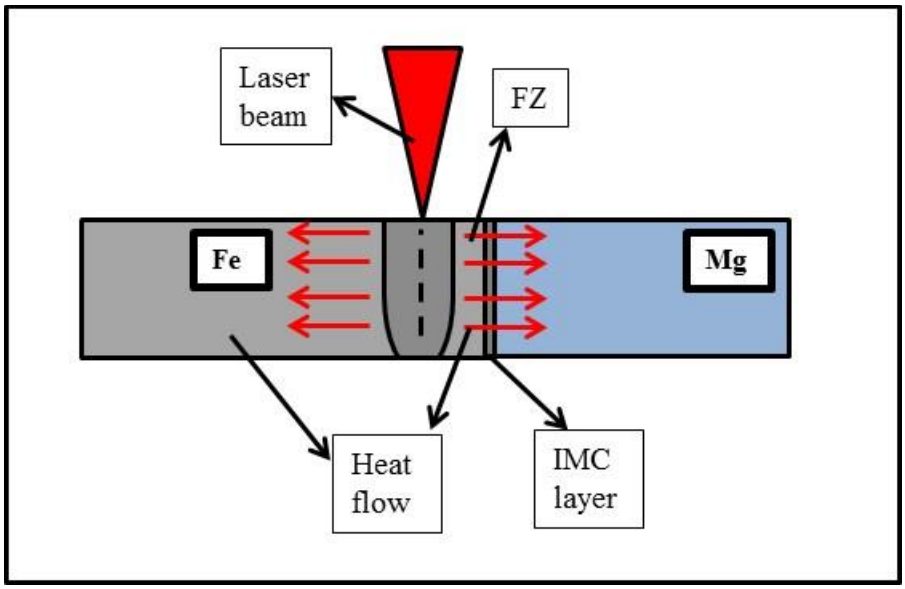


Fig.2 Schematic drawing for describing the joining mechanism by LOW technique.

2.2 Set-up of welding system

Integrated instruments were combined to accomplish the process. The whole apparatus set-up mainly comprises a laser system with multi-axes machine, a shielding gas system and a workbench, equipped with clamps and supporting table (see fig. 3). A disk Yb-YAG laser, with a wavelength of 1030 nm and a maximum available power of 10 kW, was used in continuous wave regime. The active gain medium consisted in a 200 μm diameter Yb optical fiber. Collimating lens and focusing lens with a focal length of 120 mm and 250 mm respectively were adopted for beam delivering. Preliminary tests were carried out to determine the focal plane and focal depth, in order to ensure minimum spot diameter at high energy density. Then a beam profiler was adopted to detect the spatial intensity profile at the focal plane. A focus spot of about 400 μm diameter ($1/e^2$ width) near-

Gaussian distribution was positioned on the top surface of the stainless steel sheet according to the LOW principle.

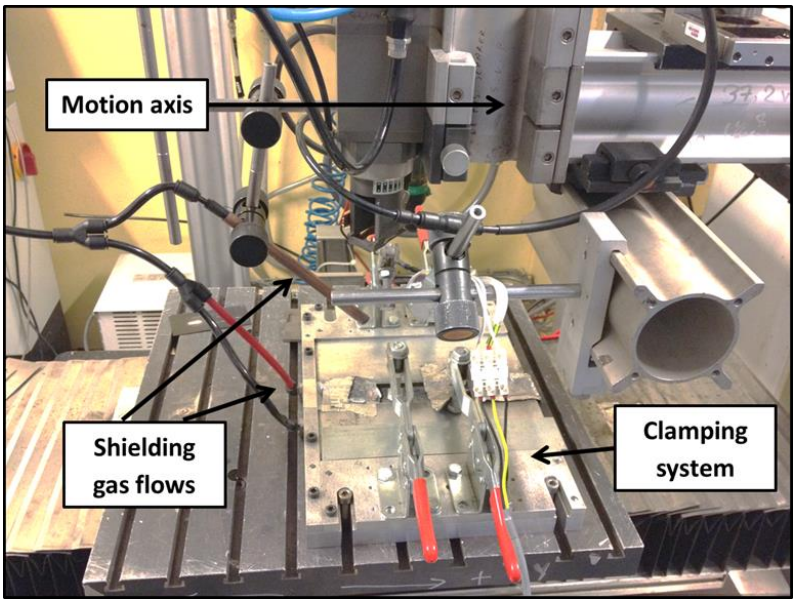


Fig. 3 LOW experimental set-up.

The sheets were fixed to the support by using four clamps. The workbench is schematically presented in figure 4.

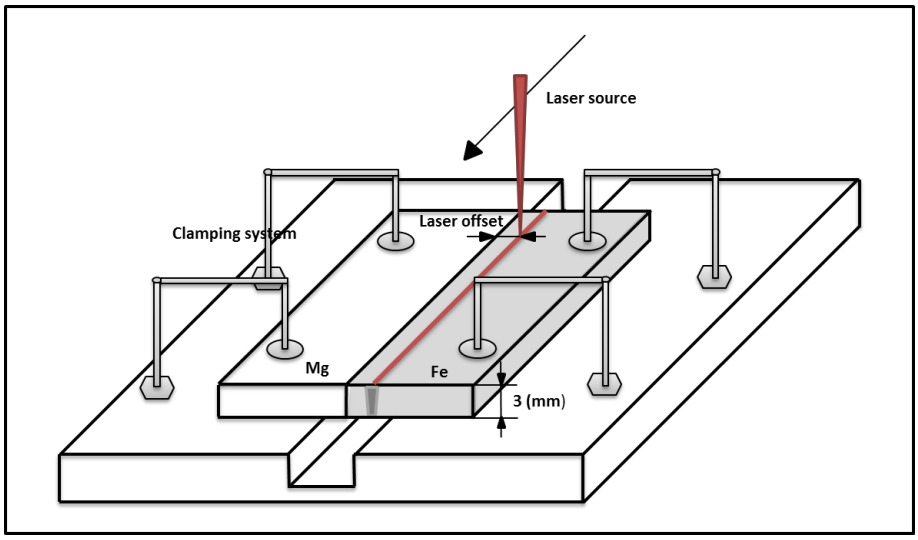


Fig. 4 Schematic drawing to overview the workbench set-up.

2.3 Plan of the experiment

Preliminary bead-on-plate tests were conducted to find suitable values of process parameters and to identify key issues that could affect the repeatability of the process. In order to reduce the thermal contact resistance, the sheets were prepared by machining at low milling speed, grinding and cleaning with acetone.

A camera inspected the gap between the sheets. It was reported an average gap of about 35 μm, which provides for a good thermal coupling. The misalignment and gaps between the sheets are critical problems during autogenous laser welding processes. This aspect is even more detrimental for dissimilar joining, in which the metallurgy could be highly sensitive to small displacements. An optimal clamping and an accurate sheet preparation could potentially minimize these concerns. High-precision cutting methods for interfaces and in situ monitoring of plates displacement could be adopted. However, in the industrial environment, the coupling between the sheets could be exasperated by other factors, including the length of the welds or the capability of the clamping system available. Furthermore, a greater accuracy in the coupling could increase the time and costs of the process. As a consequence, the present study was conducted by adopting a common clamping system, and sheets were prepared according to standard mechanical procedures, in order to approximate the feasibility of the present technique for industrial purposes.

Trial sets of experiments were performed for ensuring satisfactory penetration and avoiding lack of fusion zones. The laser power and the travel speed were kept constant at 2.5 kW and 1.8 m/min respectively. This results in a thermal input (defined as the ratio of the power to the welding speed) of about 83 J/mm. The laser offset was varied on three levels, i.e. 0.3, 0.4 and 0.5 mm, in order to explore its influence on the microstructural properties along the intermetallic layer. In fact, the specific objective of the present work is to study the weldability between magnesium alloy and stainless steel by direct laser irradiation as a function of the offset distance. Visual macro inspections and optical and electron microscopy. Both microhardness and tensile test were performed to analyse the static properties .

2.4 Metallographic analysis and mechanical testing

Metallographic specimens were prepared according to standard procedures. Samples were sectioned, mounted in a conductive resin and polished mechanically. Since the weld was made up of two different materials, a tailored procedure for chemical etching was designed, which included two steps:

- Firstly, the magnesium side was etched by immersing the whole specimen surface in a 10% aqueous solution of oxalic acid. This action did not have effect on the steel side, but provided for microstructures in the magnesium fusion zone.
- Secondly, an electrolytic polishing/etching machine (STRUERS Lectropol-5) was adopted for electrolytic etching with the same acidic solution, leading to over-etching the magnesium side (that lost contrast) and chromatic contrast in the steel side.

The microstructure was studied by optical microscopy (OM) and scansion electron microscopy (SEM). The analysis of chemical composition was carried out by Energy-dispersive X-ray spectroscopy (EDS).

Vickers micro-hardness measurements were carried out on a HighWood HWMMT-X7 hardness tester with a 200 gf load.

Tensile tests on the base material and on the joints were carried out on a universal electromechanical tensile test machine (INSTRON 4485) equipped with pneumatic grips. In order to investigate the strain behavior of the joint, all tests were assisted by an optical strain measurement system (ARAMIS by GOM), based on the digital image correlation. The image is discretized in a cells grid and the software automatically recognizes the cells during the test, calculating displacements and strains. The acquisition of local strain allows acquiring the strain value in a very small area of the specimen. Two 1.3 MPixel sensors were used with the ARAMIS strain measurement software. An acquisition rate of 1 Hz was used during the tests. Before testing,

a random black speckle pattern was applied over a previously white painted mat surface, in order to enable data acquisition by cameras.

3. MICROSTRUCTURE ANALYSIS AND MICROHARDNESS

In Fig. 5, cross sections of the joints welded with 0.3 and 0.4 mm laser offset are depicted: the fusion zone in the steel can be observed on the right portion of the image whilst the fusion zone of the magnesium alloy is on the left side. A catastrophic lack of fusion was registered for sample 3, which exhibited poor mechanical properties.

No further description will be reported on sample 3, since its outcome was not successful. Because of the excessive offset distance, the thermal energy at the interface was not sufficient to produce the weld. As a consequence, the steel weld pool collapsed and wetted the solid state magnesium. The interaction between materials in two different states just promoted a cohesive bonding without generating any phases' coalescence. This phenomena is not amongst the topics of the current investigation. Threshold limits for laser offset is a fundamental aspect that will be object of ongoing studies.

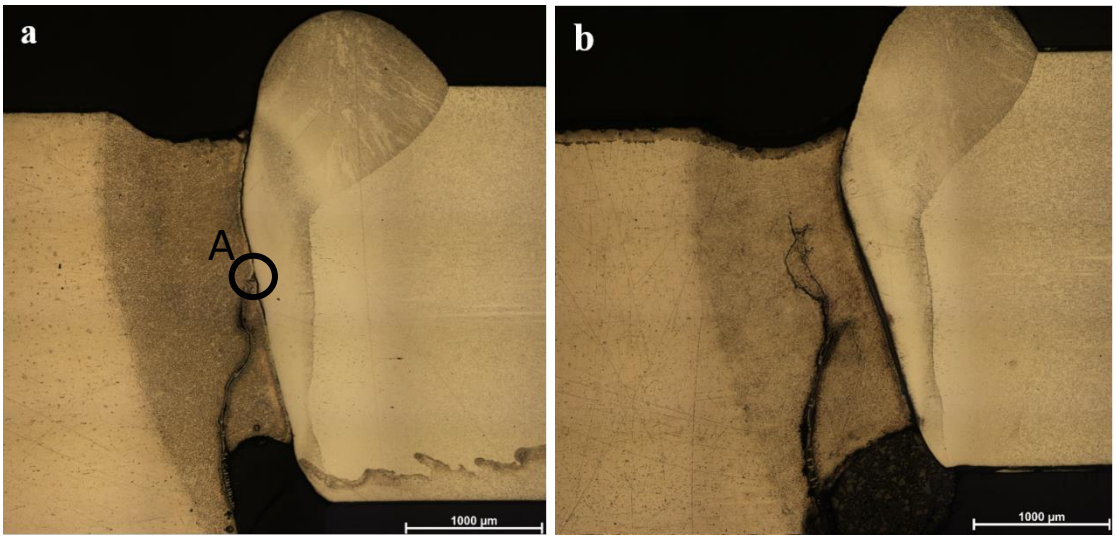


Fig. 5. Micrographs of the cross section of the AZ31-SS LOW joint. 0.3 mm offset 1 (a) and 0.4 mm offset (b).

As regards samples 1 and 2, the heat input produced a keyhole in the steel and the fusion wall reached the melted magnesium alloy. Due to the asymmetry in the heat conduction, the fusion zone of the steel moved towards the magnesium side where the interface hindered the heat conduction and made this zone overheated. In both conditions reported in Fig. 5, a pronounced excess of metal in the upper part (weld reinforcement) can be seen on the steel side. On the magnesium side (left in Fig. 5) there was a strong undercut both on the top and on the bottom of the weld bead. This weld morphology can be related to the shrinkage during the re-solidification at the liquid-liquid interface. During the heat transfer from the steel to the magnesium side, a steel downstream started from point A at the interface (figure 5a). A narrow zone due to the melt flow formed in the molten-to base-material transition zone. Figure 6 gives a close-up of the re-solidified structure. The reader can see α and β magnesium phases and interposed steel tongues.

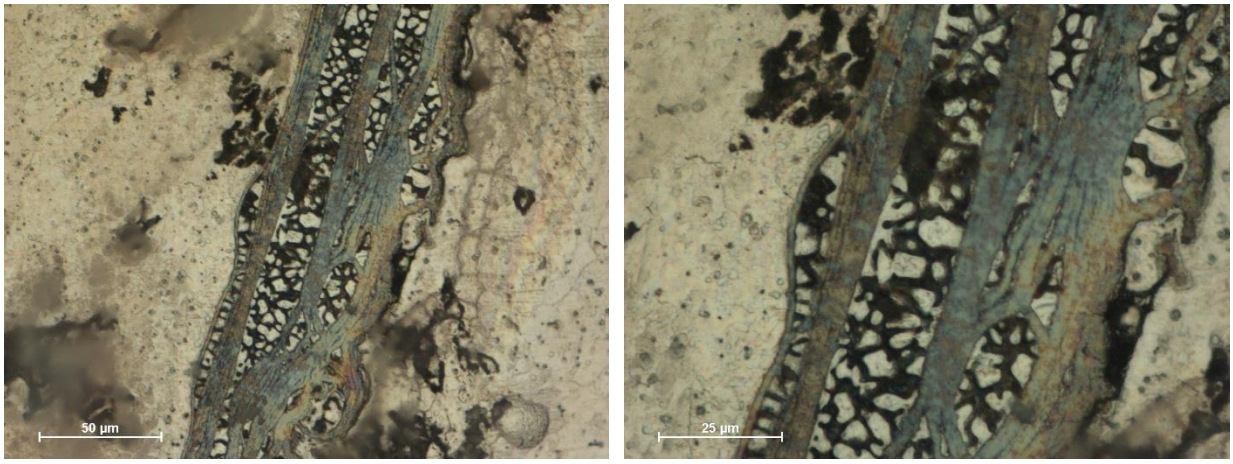


Fig. 6. Microstructure of the steel downstream in the magnesium side at two different magnification.

The same downstream structure can be observed in figure 5b, but the starting point is not in the plane of the picture. That phenomenon can be explained with overheating of some contact points between steel and magnesium, which favored the steel melt flow into the magnesium side.

In Fig. 7, results of the hardness measurement are reported. The two different conditions lead to similar hardness profiles along the weld bead.

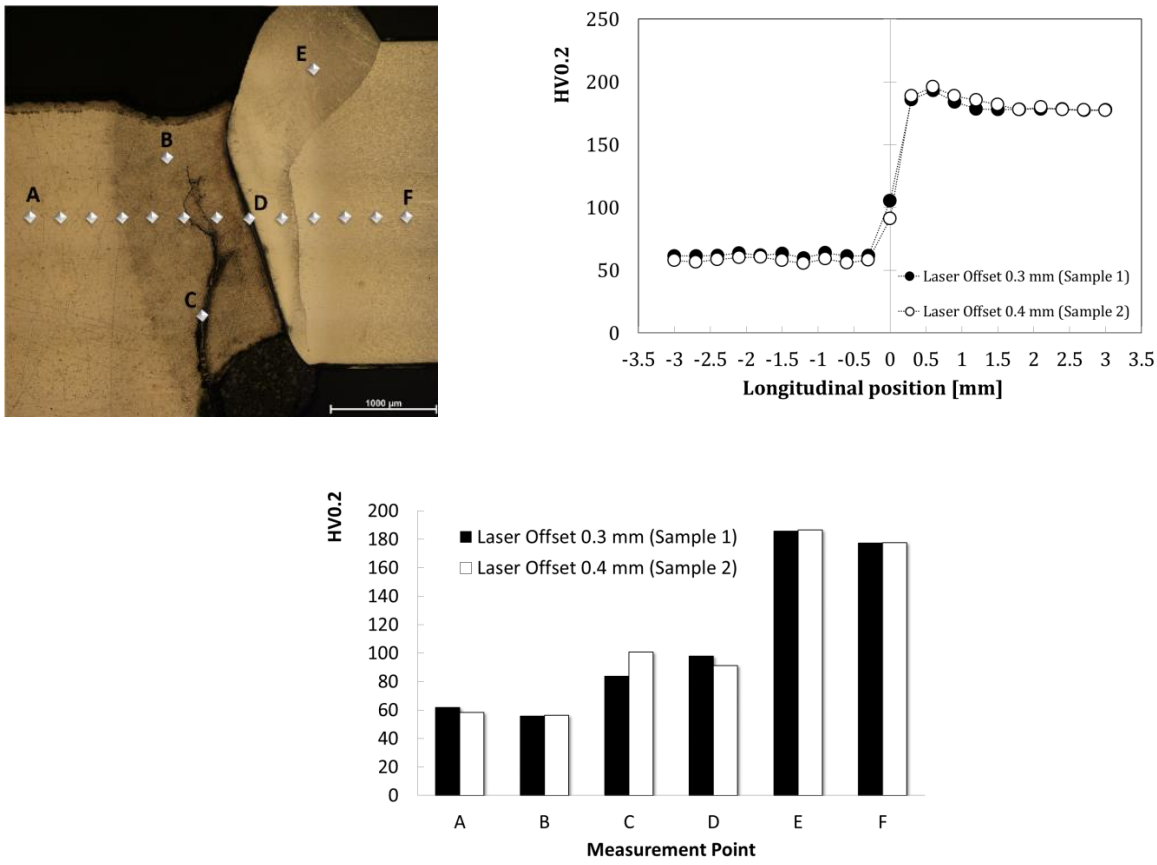


Fig. 7. Hardness profile and values along the weld in two different process conditions

The hardness in the magnesium side is almost constant and very close to the value of the base metal (approximately 56 HV). In the interface, there is a significant increase of hardness until an intermediate value between the magnesium alloy and the steel hardness. In the steel side the hardness in the fusion zone is slightly higher than that in the base metal (187 HV and 178 HV, respectively) and a peak value in the heat affected zone is found (approximately 195 HV). No significant difference between the two different welding conditions was found.

Figure 8 shows the microstructure evolution with the distance from the weld centerline.

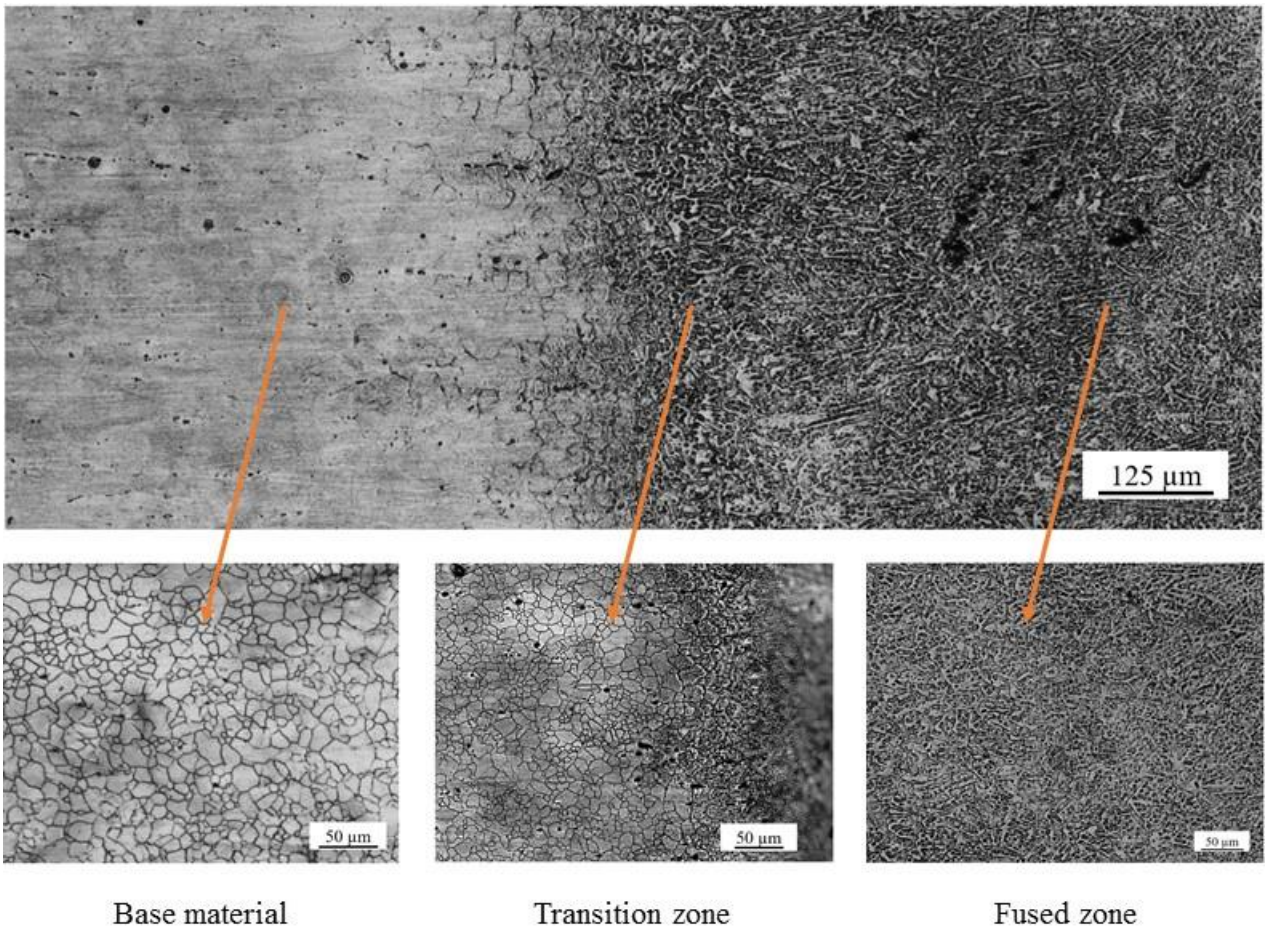


Fig. 8. Micrograph of Magnesium side with 0.4 mm offset.

During welding, a transition zone formed adjacent to the complete fusion zone. It was a partially melting zone, which was heated to the temperature range between the liquidus and solidus temperature. The grains were very small and the volume fraction of equiaxed grains accordingly increased with respect to the base material.

Many precipitates concentrated in the fusion zone, in a distribution that tended to grow from a few scattered particles to densely packed coarser ones, which is favored from the total content of Al in the Mg alloy. Al has the main influence on the formation of particles as Quan et al. (2008) explained. The coarse dendrites of primary α-Mg with the grain size of a few micrometers were observed throughout the fusion zone, which indicated a normal dendrite growth mode, by Guo et al. (2014).

In the base material, the grains are equiaxed and twins are not observed. The grain size decreased from the base material towards the fusion zone.

Figure 9 shows the intermetallic edge after welding and the eutectic, which was β-Mg_xAl_y/Mg (x and y depending on Al content), in its typical tortuous and interconnected distribution as it was explained by Wang et al. (2012).

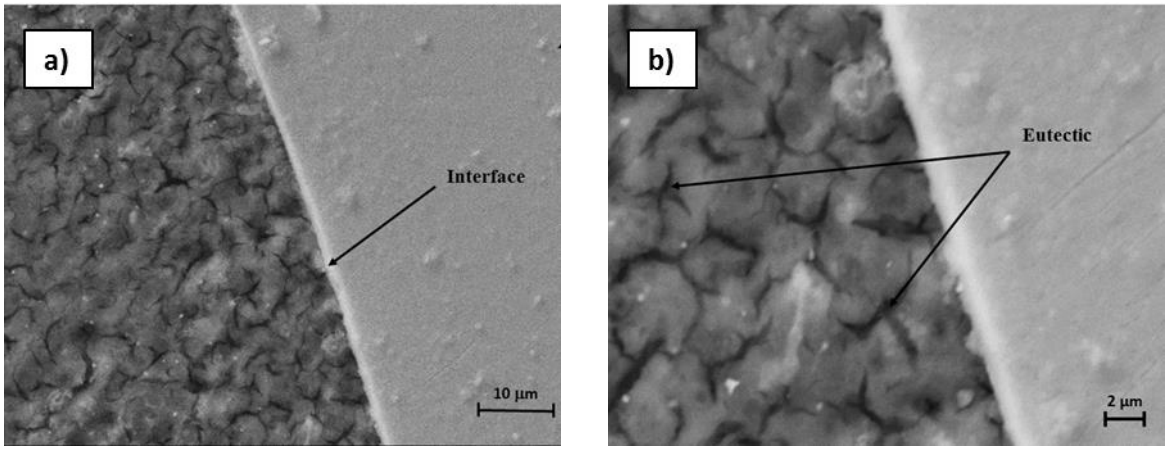


Fig. 9. Mg-steel interface (a) and evidence of the eutectic (b) at two different SEM magnification.

From a crystallographic point of view, it is not possible for pure magnesium to nucleate on steel due to the very large lattice mismatching of Fe and Mg, which has called for the use of Ni-interlayer, see Nasiri et al. (2013). A nano-interlayer probably formed (< 0.5 µm). The formation of a bond between the two alloys was probably facilitated by the deferred thermal cycle in the Magnesium side with respect to the steel one. Solid state inter-diffusion between Fe and Mg during the welding process did not occur.

The porosity in the weld, which was one of the major concerns during laser beam welding of magnesium alloys, was absent.

The loss of alloying elements at high laser power density was avoided by the irradiance incident upon the steel side of the joint.

4. TENSILE TEST

The tensile test results demonstrated that after welding, both the strength and the elongation decreased. The reduction of the tensile strength can be related to the irregular shape of the weld bead that affected the load-bearing capability during tensile testing.

The ultimate tensile strength (UTS) of the joints obtained in the 0.3 mm offset and 0.4 mm offset conditions are shown in figure 10. The sample obtained with 0.5 mm offset showed no resistance. Three samples for each condition were tested and the average UTS was also displayed.

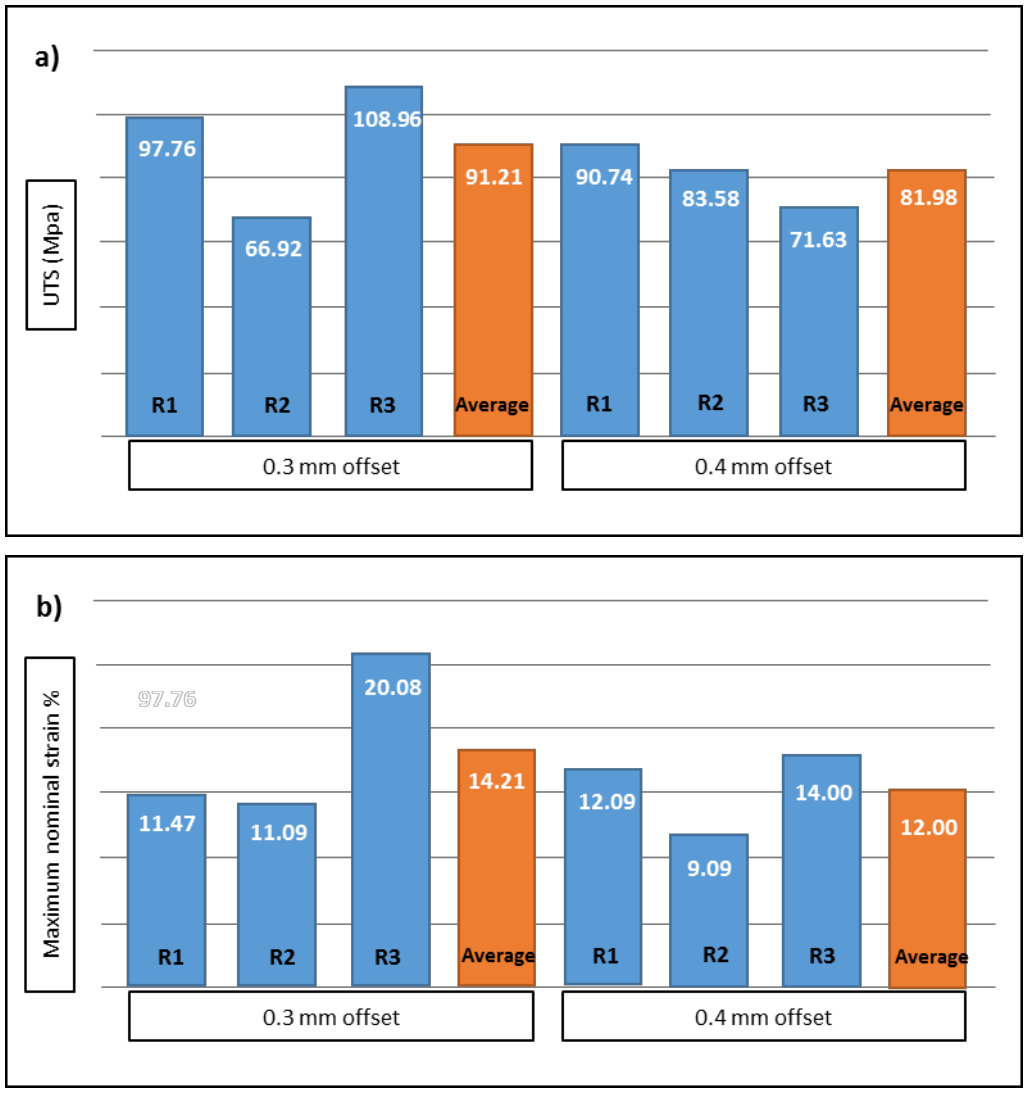


Fig. 10. Ultimate tensile strength (UTS) (a) and maximum nominal strain % (b) of the joints.

The maximum strain values in the tensile direction, registered along the area acquired by the ARAMIS system, are reported. A standard deviation of 5.08 and 2.58 mm was observed for 0.3 mm

offset and 0.4 mm offset conditions, respectively, which indicates a low dispersion of data values. In all the specimens, the maximum values were found in the welded joint and the base material underwent a low deformation.

All welds fractured in the magnesium side, quite far from the inter-layer. Figures 11 and 12 show the macro effect of fracture on the joints obtained for 0.3 and 0.4 mm offset, respectively.

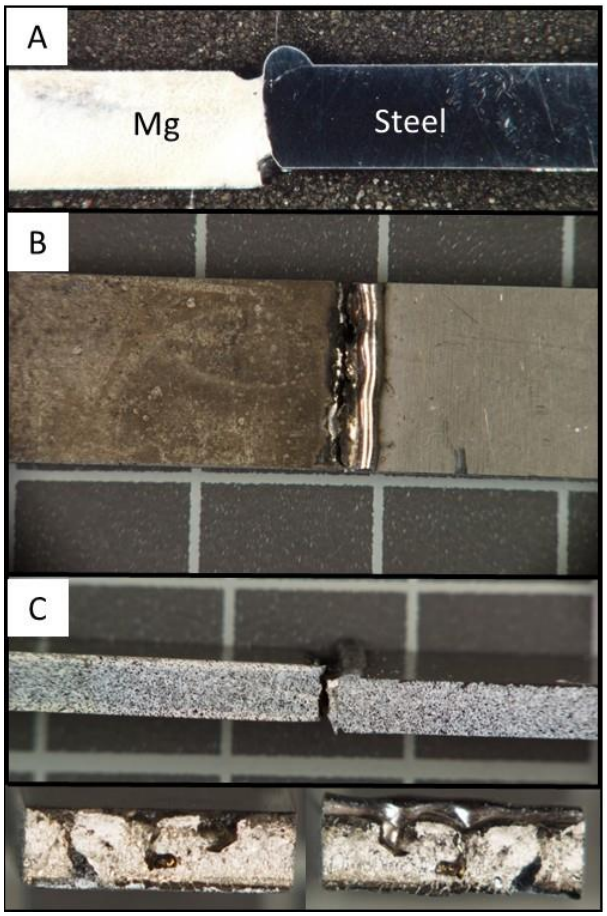


Fig. 11. Macros of the ruptured sample 1.

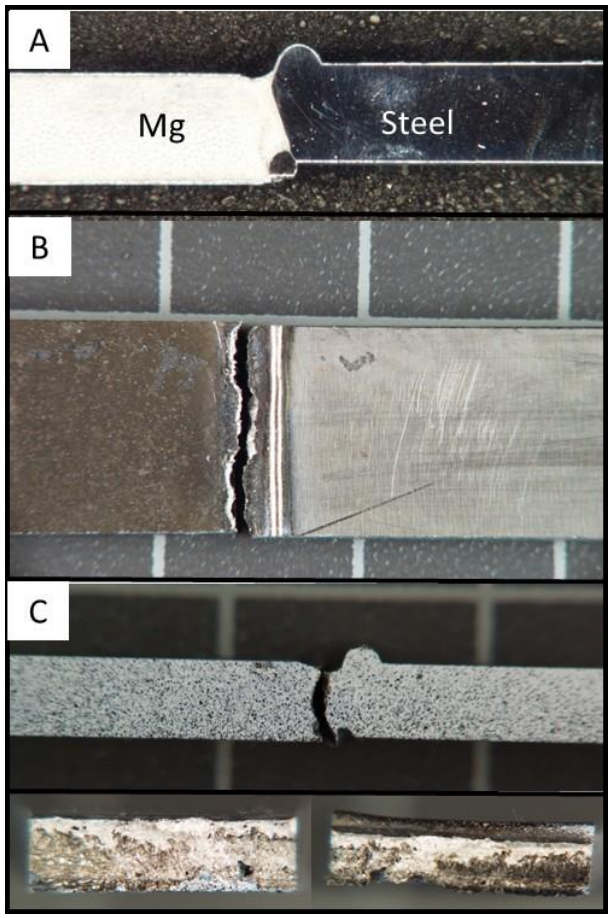


Fig. 12. Macros of the ruptured sample 2.

In figure 13, the strain profile along the middle section is reported for both the conditions analysed.

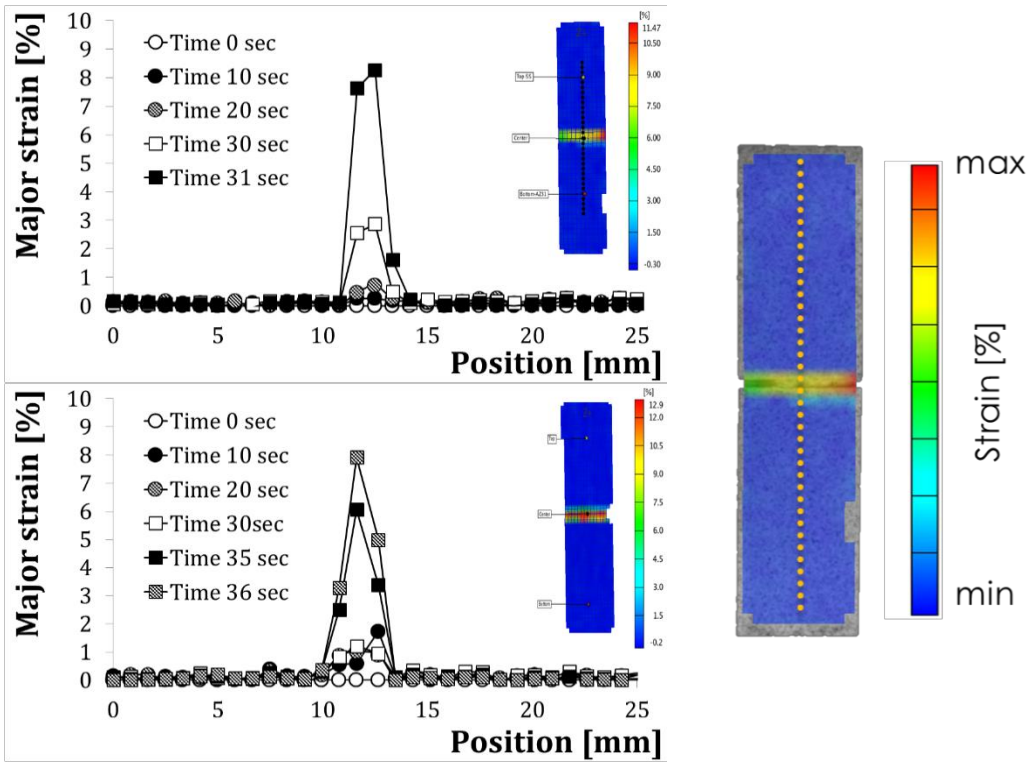


Fig. 13. Major strain profiles in different instants during the tensile test on the specimens welded at 0.3 mm offset (a) and 0.4 mm offset (b)

5. FRACTURE AND SEM ANALYSIS

Figure 14 shows a SEM image of the Mg side of the fracture surface for 0.3 mm offset.

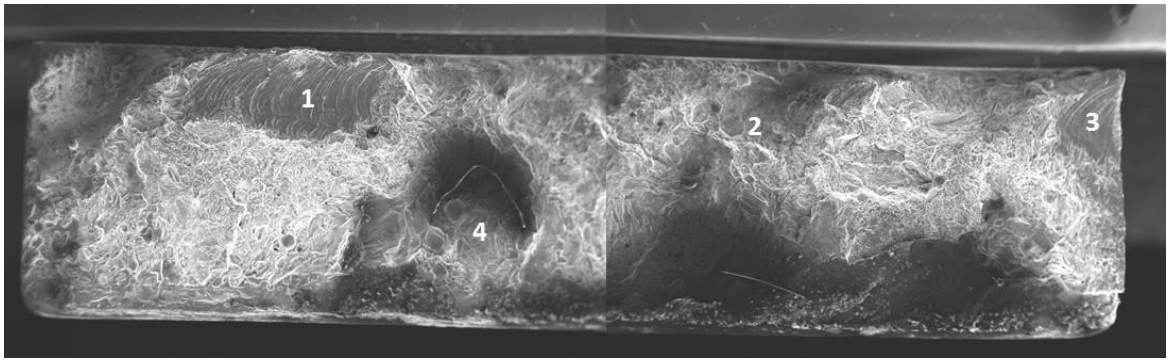


Fig. 14. Fracture surface and EDS point analysis.

SEM examinations revealed that cracks initiated from the surface or near surface welding defects at low stress (points 1 and 3 in Figure 14). Those points were characterized by lack of fusion due to under-heating. The crack propagation through the grains along several crystallographic planes caused the river marking. Then, the cracks formed plateaus and connecting ledges and stopped until the stress rose to an ultimate one. Meanwhile, the Mg deformed in a ductile manner. Eventually, the

fracture occurred with dimple-like characteristics at a relative low stress, which was due to the sub-surface defects (points 4 and 5).

Cleavage-like brittle fracture with flat facets in conjunction with river marking was also observed (figures 15 and 16). The river marking was caused by the crack propagation, see Chowdury et al. 2011.

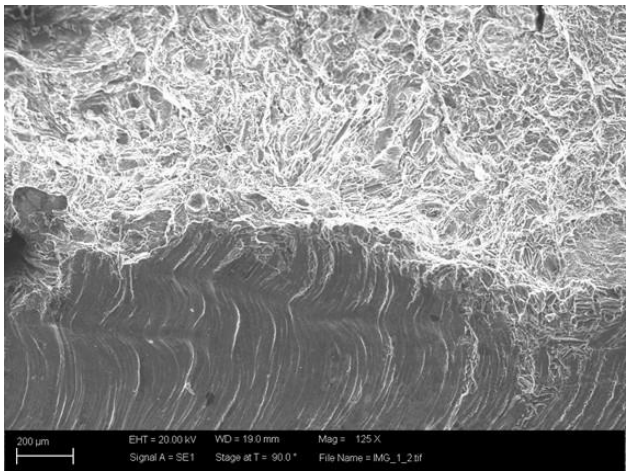


Fig. 15. Flat facets-to-dimple transition zone (125x).

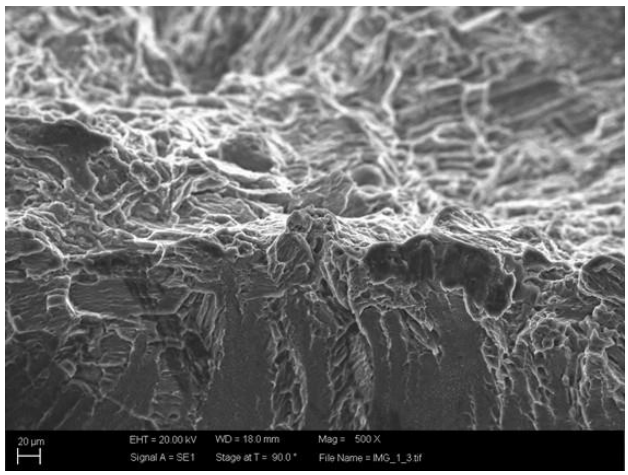


Fig. 16. Flat facets-to-dimple transition zone (500x).

The EDM analysis of some points of the fracture surface of sample 1 are shown in figures 17 to 20. The composition (wt %) of elements was also reported.

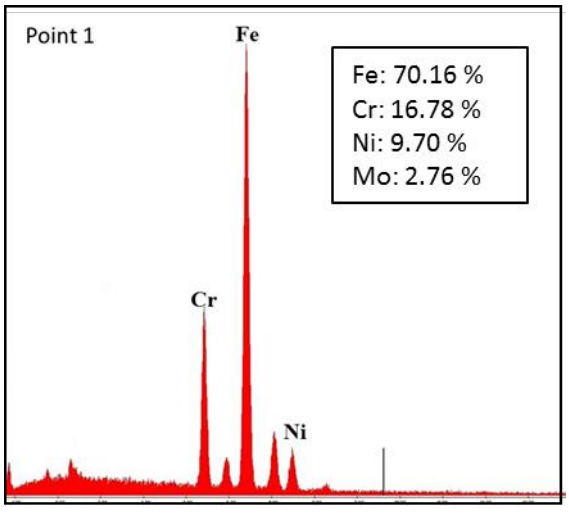


Fig. 17. Chemical composition at point 1 (figure 14)

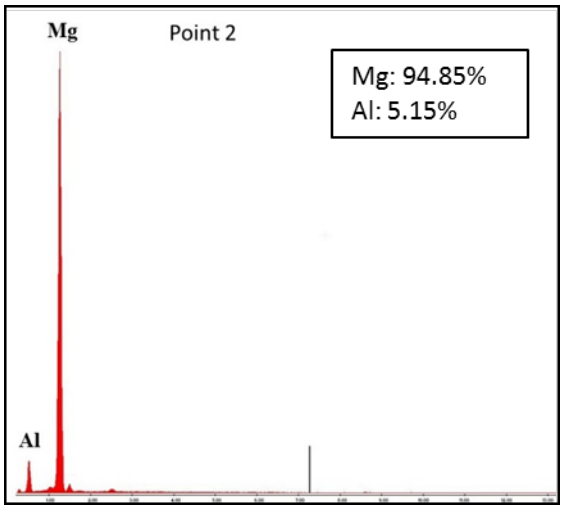


Fig. 18. Chemical composition at point 2 (figure 14)

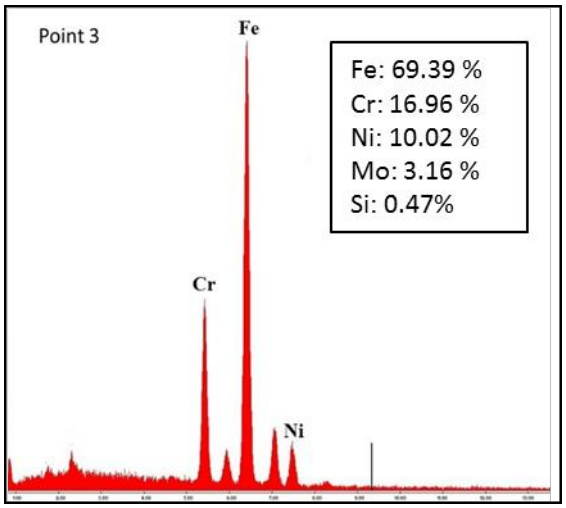


Fig. 19. Chemical composition at point 3 (figure 14)

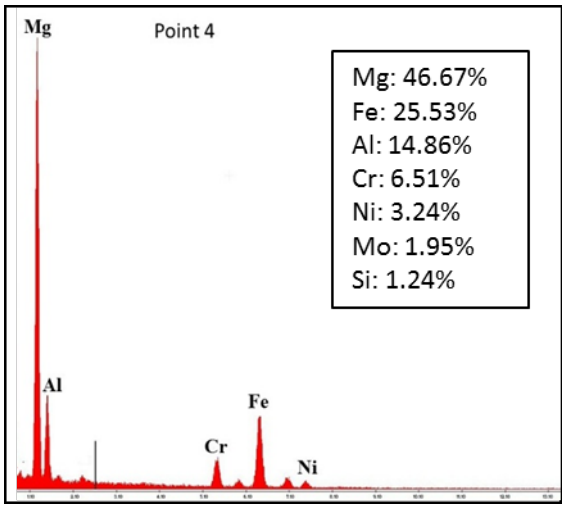


Fig. 20. Chemical composition at point 4 (figure 14)

The points 1 and 3, where Magnesium was absent, presented a cleavage-like brittle fracture. In those points, the rupture was initiated by surface defects and rapidly propagated in the magnesium side of the weld where dimple-like rupture surface was observed (points 2 and 4).

CONCLUSIONS

The study of the offset fiber laser welding of magnesium alloy AZ31 to the 316 stainless steel gave the following evidences.

- A thin layer, which dimension was in the order of micron, formed in the weld zone, without the need for any interposed interlayer. as revealed by the SEM analysis.
- Steel melt flows into the magnesium side were observed. They may depend on the contact condition between the two plates, which can induce local overheating.
- Although zones of lack of fusion and surface defects were observed on the fractured surface, the tensile test indicated that the UTS was close to 100 MPa.
- In the zone where the interlayer well formed, the rupture was ductile. A flat facets-to-dimple transition zone was observed.

- The loss of alloying elements at high laser power density was avoided, since the laser beam stroke the steel side of the joint.

As a number of drawbacks in Magnesium to stainless steel fusion laser welding were avoided without interposing any interlayer, it has been demonstrated that the LOW technique has the potential to produce the Mg-steel weld. . Future work to improve the geometry of welds should validate this statement.

References

Caiwang, T., Song, X., Meng S., Chen, B., Li, L., Feng, J., 2016. Laser welding-brazing of Mg to stainless steel: joining characteristics, interfacial microstructure, and mechanical properties. Int J Adv Manuf Technol., 86, 203–213.

Casalino, G, Campanelli, S.L., Ludovico, A.D., 2013. Laser-arc hybrid welding of wrought to selective laser molten stainless steel. Int J. Adv Manuf Technol 68:209–216.

Casalino, G., Mortello, M., Peyre, P., 2015. Yb–YAG laser offset welding of AA5754 and T40 butt joint. J Mater Process Technol 223:139–149.

Chen H.C., Pinkerton A.J., Li L., 2011. Fibre laser welding of dissimilar alloys of Ti-6Al-4V and Inconel 718 for aerospace applications. Int J Adv Manuf Technol, 52, 977–987.

Chen, Y.C., and Nakata, K., 2009. Effect of tool geometry on microstructure and mechanical properties of friction stir lap welded magnesium alloy and steel. Materials & Design, vol. 30, pp. 3913–3919.

Chen, Y.C., and Nakata, K., 2010. Effect of surface states steel on microstructure and mechanical properties of lap joints of magnesium alloy and steel by friction stir welding. Science and Technology of Welding and Joining, 15:4, 293-298.

Chowdury, S.M., Chen, D.L., Bhole, S.D., Powidajko, E., Weckman, D.C., Zhou, Y., 2011. Microstructure and Mechanical Properties of Fiber-Laser-Welded and Diode-Laser-Welded AZ31 Magnesium Alloy. Metallurgical and Materials Transaction A, 42A, 1974-1989.

Elthalabawy W. M., Tahir I. K., 2011.Eutectic bonding of austenitic stainless steel 316L to magnesium alloy AZ31 using copper interlayer International Journal of Advanced Manufacturing Technology, vol. 55, 235-241.

Guo, H.M., Zhang, A.S., Yang, X.J., Yan, M.M., Ding, Y. 2014. Microstructure Formation and Mechanical Properties of AZ31 Magnesium Alloy Solidified with a Novel Mechanical Vibration Technique. Metallurgical and Materials Transactions A, 45, 438–446.

Jana S., Hovanski Y., Grant G.J., 2010. Friction stir welding of magnesium alloy to steel: a preliminary investigation. Metallurgical and Materials Transaction A, 41(A), 3173-3182.

Liu, L., Xiao, L., Feng, J.C., Tian, Y.H., Zhou, S.Q., Zhou Y., 2012. The Mechanisms of Resistance Spot Welding of Magnesium to Steel. Metallurgical and Materials Transaction A, 41(A), 2651-2661.

Liu, L.M., Qi, X., Wu, Z., 2010. Microstructural characteristics of lap joint between magnesium alloy and mild steel with and without the addition of Sn element. Materials Letter, 64, 89–92.

Nasiri, A. M., Weckman, D. C., Zhou, Y. 2013. Interfacial Microstructure of Diode Laser Brazed AZ31B Magnesium to Steel Sheet Using a Nickel Interlayer. Welding Journal, 92, 1s-10s

Nasiri, A.M., Weckman, D.C., Zhou, Y., 2015. Effect of Zn interlayer on brazeability of AZ31B-Mg alloy to steel sheet. Welding Journal, 94, Issue 3, 1 Pages 61s-72s.

Nasiri, A.M., Zhou, Y., 2015. Interfacial microstructure of laser brazed AZ31B magnesium to sn-plated steel sheet: Brazeability, interfacial microstructure, and mechanical properties were investigated. Science and Technology of Welding and Joining, 20, 155-163.

Quan, Y., Chen, Z., Gong, X., Yu, Z., 2008. CO_2 laser beam welding of dissimilar magnesium-based alloys. Materials Science and Engineering A, 496, 45–51.

Saha R. K. and Khan T. I., 2006. Effect of bonding temperature on transient liquid phase bonding behavior of a Ni-based oxide dispersion-strengthened superalloy. Journal of Materials Engineering and Performance, 15, 722–728.

Saha R. K. and Khan T. I., 2009. Microstructural developments in TLP bonds using thin interlayers based on Ni–B coatings. Materials Characterization, 60, 1001–1007.

Tan, C. W., Li, L. Q., Chen, Y. B., Nasiri, A.M., Zhou, Y., 2014. Microstructural Characteristics and Mechanical Properties of Fiber Laser Welded Brazed Mg Alloy Stainless Steel Joint. Welding Journal, October 93, 399s-409s.

Tomashchuk, I., Sallamanda, P., Cicala, E., Peyre, P., Grevey, D., 2015. Direct keyholelaser welding of aluminum alloy AA5754 to titanium alloy Ti6Al4V. J. Mater.Process. Technol. 217, 96–104.

Wahba, M., and Katayama, S., 2012. Laser welding of AZ31B magnesium alloy to Zn-coated steel. Materials & Design, 35, 701-706.

Wang, M. Y., Williams, J. J., Jiang, L., De Carlo, F., Jing, T., Chawla, N., 2012. Three Dimensional (3D) Microstructural Characterization and Quantitative Analysis of Solidified Microstructures in Magnesium-Based Alloys. Metallogr. Microstruct. Anal. 1, 7–13.

Wei Y., Li J., Xiong J., Zhang F., 2012. Microstructures and mechanical properties of magnesium alloy and stainless steel weld-joint made by friction stir lap welding. Materials and Design 33(1):111-114.

Yuan X., Sheng G., Luo J., Li J., 2013. Microstructural characteristics of joint region during diffusion-brazing of magnesium alloy and stainless steel using pure copper interlayer. Trans. Nonferrous Met. Soc. China, 23, 599−604.



https://dspace.org/

Laser offset welding of AZ31B magnesium alloy to 316 stainless steel

Casalino, G.; Guglielmi, P.; Lorusso, V. D.; Mortello, Michelangelo; Peyre, P. ...

2016-11-18
Elsevier
http://dx.doi.org/10.1016/j.jmatprotec.2016.11.020
Casalino G, Guglielmi P, Lorusso VD, Mortello M, Peyre P, Sorgente D, Laser offset welding of AZ31B magnesium alloy to 316 stainless steel, Journal of Materials Processing Technology, Volume 242, April 2017, Pages 49–59

Downloaded from a DSpace repository. https://dspace.org/